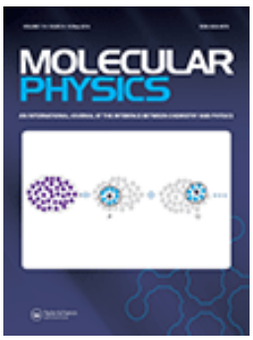

Taylor & Francis
Taylor & Francis Group

Molecular Physics

An International Journal at the Interface Between Chemistry and Physics

ISSN: 0026-8976 (Print) 1362-3028 (Online) Journal homepage: http://www.tandfonline.com/loi/tmph20

Continuous version of a square-well potential of variable range and its application in molecular dynamics simulations

I. M. Zerón, C. Vega & A. L. Benavides

To cite this article: I. M. Zerón, C. Vega & A. L. Benavides (2018): Continuous version of a square-well potential of variable range and its application in molecular dynamics simulations, Molecular Physics, DOI: 10.1080/00268976.2018.1481232

To link to this article: https://doi.org/10.1080/00268976.2018.1481232

Published online: 14 Jun 2018.

MOLECULAR PHYSICS
https://doi.org/10.1080/00268976.2018.1481232

Taylor & Francis
Taylor & Francis Group

FRENKEL SPECIAL ISSUE

Continuous version of a square-well potential of variable range and its application in molecular dynamics simulations

I. M. Zerón[a], C. Vega[b] and A. L. Benavides[a]

[a]División de Ciencias e Ingenierías, Universidad de Guanajuato, Guanajuato, México; [b]Depto. Química Física I, Fac. Ciencias Químicas, Universidad Complutense de Madrid 28040, Madrid, Spain

ABSTRACT

In this work, we present a simple mathematical expression for a continuous version of the square-well (SW) discontinuous potential of variable range ($\lambda \geq 1.05$). This expression can be useful in theoretical statistical mechanics methods and specially in conventional molecular dynamics (MD) simulations. To illustrate the latter point, the continuous version of some SW potentials of variable range were selected and studied with continuous MD. SW single state thermodynamic and structural properties (vapour, liquid and solid), vapour–liquid phase diagrams and surface tensions accurately reproduce available simulation data obtained by Monte Carlo and discontinuous MD simulation methods. This expression can be easily implemented in popular simulation packages (GROMACS, NAMD, CHARMM, DL_POLY, EXPResSo, HOOMD, TINKER, ls1 mardyn, etc.) that can be useful to study more complex systems. Besides we also present a continuous version for the square-shoulder potential.

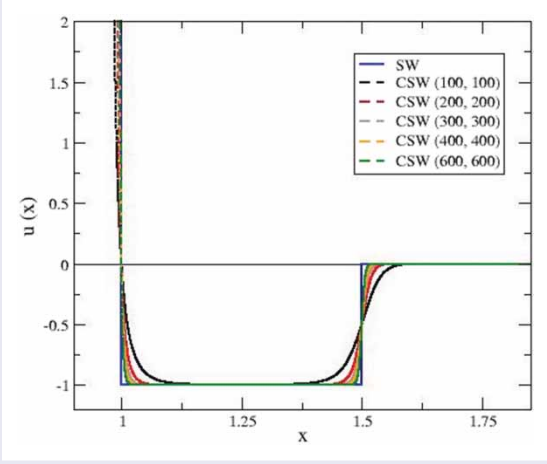

ARTICLE HISTORY
Received 17 January 2018
Accepted 12 May 2018

KEYWORDS
Molecular dynamics simulation; continuous square-well potential; continuous square-shoulder potential

1. Introduction

In Statistical Mechanics, hard-sphere (HS), square-well (SW), square-shoulder (SS) potentials and some of their combinations (discrete potentials) have been used as toy models in the context of fluids due to their mathematical simple expressions. Discrete potentials simplify the calculus of terms that appear in the evaluation of Virial Coefficients, Perturbation Theory and Integral Equations Methods [1–18]. Although they are simple and discontinuous potentials, they have been used as effective models for real systems, such as in the modelling of colloids [19–22] and proteins [23–25]. The SS potential does not exhibit a vapour–liquid transition; however, it has a very reach fluid–solid and solid–solid phase diagrams. It has been shown that this potential predicts that particles can self-organise in highly complex, low-symmetry lattices, forming clusters, columns or lamellae, and at high pressures they form compact and high-symmetry structures [26,27]. A very interesting application has been recently presented by Pattabhiraman et al. [28] using the SS model potential while designing photonic crystals. Besides stripe patterns have been observed for

CONTACT A. L. Benavides alb@fisica.ugto.mx División de Ciencias e Ingenierías, Universidad de Guanajuato, Loma del Bosque 103, Colonia Lomas del Campestre, CP 37150 León, Guanajuato, México

two-dimensional SS potentials [29–31]. In two dimensions, SW potentials also exhibit a variety of different phases: vapour, liquid, hexatic and triangular solid and a non-compact solid with square-lattice symmetry [32].

Simulation studies for discrete potentials have been mostly performed with Monte Carlo (MC) techniques [33–54]. Due to their discontinuities, these kinds of potentials have not been treated by conventional molecular dynamics (MD) simulation that is a very important technique that has been applied to many continuous potentials and successfully incorporated in more general popular simulation packages (GROMACS [55–61], CHARMM [62], DL_POLY [63], EXPResSo [64], IMD [65], LAMMPS [66], ls1 mardyn [67], NAMD [68], TINKER [69], HOOMD [70,71], etc.) to study a great variety of complex systems. Besides, MD simulation has the advantage over the MC method that one can obtain the transport properties of a given potential.

The discontinuous molecular dynamics (DMD) [32,44,72–75] is an alternative simulation method that avoids solving the Newton equations for model potentials with discontinuous forces. Instead they solve collisions among particles while obeying the conservation of energy and momentum of the system. However, the DMD method has not been implemented until recently to standard simulation packages for event-driven MD [76], and its use has been mostly limited to homemade simulation programs in the context of particular problems.

A way of avoiding the difficulties of treating hard-core potentials with MD simulations is the constant force approach method proposed by Orea and Odriozola [77]. This method consists in replacing the hard-core discontinuity by a very steep linear function whose derivative is a constant. The extension to a potential with more than one discontinuities has been recently done by Padilla and Benavides [78] and results for discrete potentials are promising.

Another way of handling the discontinuity of the HS potential in many MD simulations has been done replacing it by continuous functions of the form $1/r^n$, with n being an integer whose value is around 60. An improved continuous version of an HS potential was developed by Jover et al. [52]. They proposed a continuous version of the HS potential, the so-called pseudo-HS potential, that is a cut and shifted version of a Mie potential with exponents (50,49). They have been able to accurately reproduce structural and thermodynamic properties when compared with available simulation data for the original HS system. Besides, the pseudo-HS potential has been successfully applied to study the liquid–solid coexistence using the MD direct coexistence method [79].

Other discontinuous potentials that have been expressed as continuous functions to be studied by MD simulations are the SS [80,81], the discrete potential made of an SS plus an SW potential (SS+SW) by Franzese [82] and the smooth version of the Jagla potential, the Fermi-Jagla potential [83].

In this work, we will provide an analytic continuous expression for an SW potential of variable range that can be used in conventional MD simulations. We describe the details of this potential in Section 1. MD simulation details are given in Section 2. Results of thermodynamic and structural properties and vapour–liquid phase diagrams for SW potentials of ranges $\lambda = 1.25$, 1.5 and 2.0 are presented in Section 3 and compared with the available SW simulation data. As a corollary we present a continuous version of the SS potential. Finally, in Section 4 we give the main conclusions of this study.

2. Continuous SW potential

The simplest model of a fluid whose particles interact with repulsive and attractive forces is the SW potential, U_{SW}, that in reduced units can be expressed as

$$u_{SW}(x) = \begin{cases} \infty & 0 < x \leq 1, \\ -1 & 1 < x \leq \lambda, \\ 0 & x > \lambda, \end{cases} \tag{1}$$

where $u_{SW}(x) = U_{SW}(x)/\epsilon$, ϵ is the depth of the SW potential, $x = r/\sigma$ the reduced interparticle distance, σ the molecular diameter and λ the SW potential range.

A continuous version of the reduced SW potential, hereafter referred as continuous square-well (CSW) potential, takes the form:

$$u_{CSW}(x) = \frac{1}{2}\left(\left(\frac{1}{x}\right)^n + \frac{1 - \mathrm{e}^{-m(x-1)(x-\lambda)}}{1 + \mathrm{e}^{-m(x-1)(x-\lambda)}} - 1\right), \tag{2}$$

where n and m are free parameters characterising the softness of the repulsive and attractive parts of the potential, respectively. The CSW potential is continuous over all domains. By construction this potential is zero in $x = 1$; it has only one minimum (-1) in approximately $x = (\lambda + 1)/2$. Moreover, the reduced CSW force, $f_{CSW} = F_{CSW}\sigma/\epsilon$, is also continuous as is required in traditional MD simulations:

$$f_{CSW}(x) = \frac{n}{2}\left(\frac{1}{x}\right)^{n+1} - \frac{m(2x - \lambda - 1)\mathrm{e}^{-m(x-1)(x-\lambda)}}{(1 + \mathrm{e}^{-m(x-1)(x-\lambda)})^2}. \tag{3}$$

For all cases considered in this work, the exponents were selected, $n = 2500$ and $m = 20000$ (see Figure 1). These such big exponent values reproduce the expected natural form of a continuous version of the potential and force simultaneously for SW potentials of ranges $\lambda \geq 1.05$. Besides for these selected values the potential tends

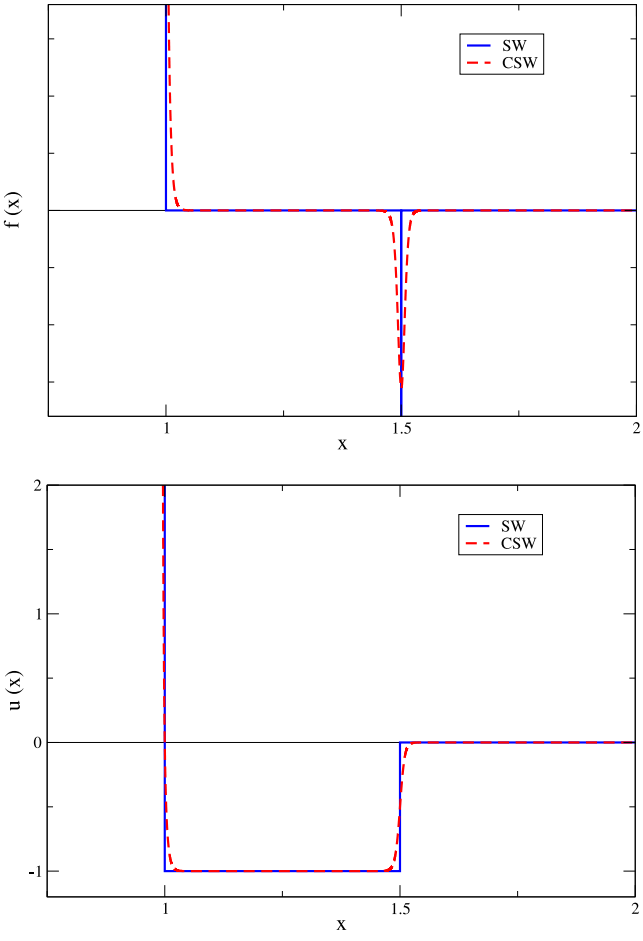

Figure 1. CSW and SW potentials for the case of SW range $\lambda = 1.5$. In the top panel, the potentials are shown and, in the bottom panel, their corresponding forces as a function of the interparticle distance x. In this figure, we have used $n = 400$ and $m = 400$ to amplify the softness of the CSW potential since for the exponent values used in this work ($n = 2500$ and $m = 20000$) the CSW and SW potentials are almost identical in the scale of the plot.

to zero at a slightly greater distance than the SW range. The same expression, Equation (2), can still be used for smaller ranges ($1 < \lambda < 1.05$) but using higher values for n and m. The continuous HS case is only recovered in the limit when $\lambda \to 1$ and $m \to \infty$.

3. Simulation details

We performed MD simulations by using the GROMACS package version 5.1. We have chosen argon simulations with particle diameter $\sigma = 0.3405$; nm, energy minimum $\epsilon = 0.996078$; kJ/mol and atomic mass $m = 39.948$ u. Although this package can be used for well-known continuous potentials, such as Lennard-Jones, Coulomb and Buckingham potentials, it can also be used for other types of interactions that can be presented in an input table with a very fine discretization. We have done this for the CSW potential with an spacing gap of 0.00001 nm to reproduce the continuous force minimum. In contrast to the SW potential that has a fixed range, for the CSW potential it is necessary to define a cut-off distance. In GROMACS distance units, it was chosen at the distance for which the potential has an approximated value $U_{CSW}(r_c) \approx 10^{-15}$ kJ/mol. For instance, for a CSW potential of range $\lambda = 1.5$, the cut-off is $r = 0.512$ nm (approximately 1.504σ) with $n = 2500$ and $m = 20{,}000$. This criterion for defining the CSW range slightly overestimates the corresponding SW range. We will refer to a CSW potential of a given range λ that corresponds to the SW range that we want to mimic, although the CSW has a slightly greater range. We included in Appendix 1 the program in Fortran that can make the GROMACS input file *table_Ar_Ar.xvg*.

In all NVT simulations, the leap-frog integrator algorithm [84], the Nosé–Hoover thermostat [85] (coupling constant $\tau = 2$ ps) and a time step $\delta t = 0.0001$ ps were used. In Appendix 2, we give a brief analysis of the time step selection according to the n and m values.

Periodic boundary conditions in all directions and a neighbour list to speed up the calculation were implemented.

To compare with the available simulation data, our results will be presented in the following reduced units: density $\rho^* = \rho\sigma^3$, temperature $T^* = k_B T/\epsilon$, excess internal energy $u = U/NkT$, reduced pressure $P^* = P\sigma^3/\epsilon$ and compressibility factor $Z = P^*/\rho^* T^*$.

Supercritical state properties were calculated from NVT simulations with a starting crystalline array conformed by 1000 particles. To equilibrate the system, 2×10^6 time steps were used and to take averages 2×10^7 steps divided into 10 sub-blocks.

To calculate the vapour–liquid coexistence, we have carried out NVT simulations in a parallelepiped simulation box with $L_z > L_x = L_y$ [86,87]. We started with a cubic crystalline array with 2000 particles at a reduced density $\rho^* = 0.8$, and the liquid state at the desired temperature is reached after 10^6 steps.

Subsequently, L_z was elongated with the ratio $L_z/L_x = 4$ where $L_x \approx 13.57\sigma$, and a second simulation was performed with 4×10^7 steps in order to allow the phase separation. The coexistence densities were obtained from the density profiles $\rho(z) = \langle N(z)\rangle/\delta V$, where $\langle N(z)\rangle$ is the average number of molecules within a slab of volume δV calculated every 10,000 steps in each slab of volume $\delta V = L_x \times L_y \times (L_z/500)$.

Extended simulations were employed (2×10^8 steps) to determine the surface tension and results were computed via the components of the pressure tensor:

$$\gamma^* = \frac{L_z^*}{2}\left[\langle P_{zz}^*\rangle - \frac{1}{2}(\langle P_{xx}^*\rangle + \langle P_{yy}^*\rangle)\right], \qquad (4)$$

where $\gamma^* = \gamma\sigma^2/\epsilon$ is the reduced surface tension, $L_z^* = L_z/\sigma$, and $\langle P_{xx}^* \rangle$, $\langle P_{yy}^* \rangle$ and $\langle P_{zz}^* \rangle$ are the average components of the pressure tensor in the x, y and z directions, respectively.

4. Results

4.1. Single-state properties

We will test the performance of the CSW against SW available simulation data.

As a first test of the CSW potential, we have carried out single-state NVT simulations for the most famous case studied in the context of simple fluids, $\lambda = 1.5$, at supercritical states (SW potential of range $\lambda = 1.5$ has a reduced critical temperature value around 1.22 [36,38,40,41]). In Figure 2, CSW potential reduced internal energies and compressibility factors as a function of temperature, $u(T^*)$ and $Z(T^*)$, for $\rho^* = 0.8$ are presented. As can be seen the CSW predictions are in good agreement with SW simulation data reported by Labík et al. [39].

For colloids models it is also important to consider cases of shorter ranges [24,88,89], so we also compared the reduced excess internal energies for a CSW potential of range $\lambda = 1.25$ at $\rho^* = 0.6$ for several supercritical temperatures (the critical temperature $T_c^* \approx 0.76$ [36,41]), and these are presented in Figure 3. Although the Patel et al. [47] reported values have large errors (not shown in this figure), our simulation data are in agreement with their central values.

In order to compare the structural properties of CSW and SW potentials, we have calculated the radial distribution function $g(x)$. As can be seen from Figure 4, the CSW potential reproduces the structural behaviour of an equivalent SW potential of range $\lambda = 1.5$ at $T^* = 2.0$ and $\rho^* = 0.8$, as reported by Henderson et al. [33], including the contact values.

To test the performance of this CSW potential in the fcc solid phase, we present in Table 1 a comparison of the internal energy and pressure predicted for an SW of range $\lambda = 1.5$ by Young and Alder [90]. As can be seen the agreement of the pressures is quite reasonable, considering that in MC simulation the pressures are indirectly obtained through extrapolations of the contact values of the radial distribution functions. For the internal energies, the agreement is very good. The errors in the internal energies and pressures were estimated calculating the standard deviation of the average properties of five independent simulation runs.

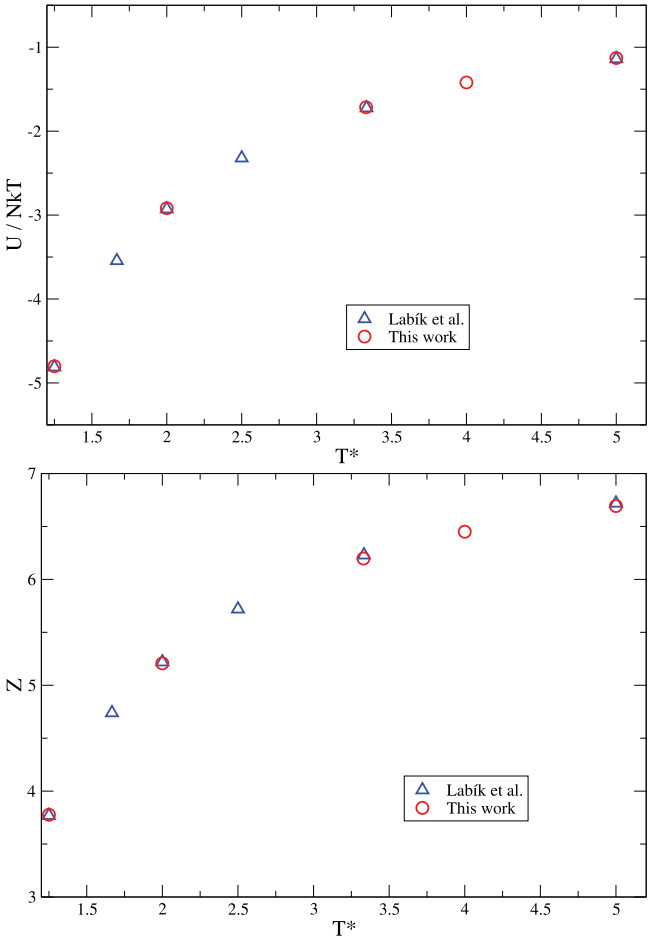

Figure 2. Supercritical excess internal energy, U/NkT (top) and compressibility factor, Z (bottom) as a function of reduced temperature for the CSW potential of range $\lambda = 1.5$ at a reduced density $\rho^* = 0.8$. Results of this work are shown with circles and with triangles the SW MC simulation data from [39].

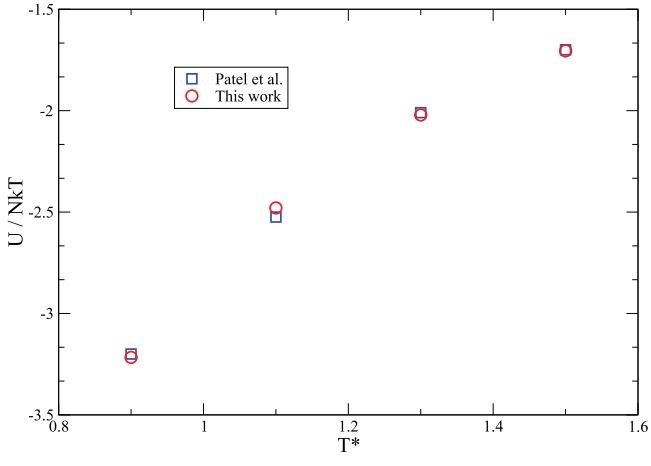

Figure 3. Internal energies for a CSW potential of range $\lambda = 1.25$ at $\rho^* = 0.6$ for several supercritical temperatures obtained in this work (circles). Simulation central data (squares) from [47] are also included. Our simulation error bars are smaller than the symbol size used.

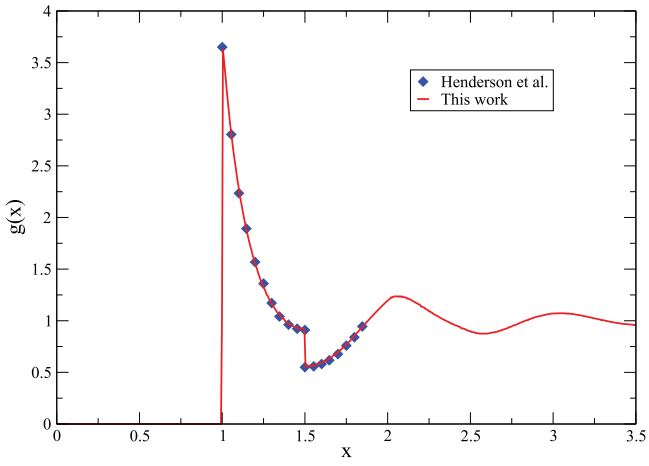

Figure 4. CSW potential radial distribution function for the case $\lambda = 1.5$ at temperature $T^* = 2.0$ and reduced density $\rho^* = 0.8$. Continuous lines are predictions from this work and filled diamonds are SW MC results from [33].

Table 1. Comparison of SW ($\lambda = 1.5$) and CSW reduced pressures and internal energies in the solid phase (fcc structure) at a reduced density $\rho^* = 1.285649$ for three different temperatures.

Potential	T^*	P^*	$U/N\epsilon$
SW	0.7	18.55	−8.95
CSW	0.7	18.82 (8)	−8.93 (1)
SW	1.0	29.47	−8.92
CSW	1.0	29.61 (11)	−8.89 (1)
SW	2.0	68.65	−8.87
CSW	2.0	68.17 (14)	−8.79 (1)

Note: The SW results are from [90].

4.2. Vapour–liquid coexistence

NVT simulations were carried out to compute the vapour–liquid coexistence densities for several temperatures for a system of particles interacting with the CSW potential (Equation (2)) with ranges $\lambda = 1.25, 1.5, 1.75$. In Table 2, the simulation data for liquid and vapour coexistence densities are presented.

The orthobaric densities were obtained from the density profiles along the z^* axis, and in Figure 5, the distribution is shown for a CSW potential of range $\lambda = 1.5$ for temperatures in the interval [0.8, 1.15]. The highest temperature was simulated with 5000 particles, instead of 2000, to have a liquid slab of similar size. In Figure 6, a good agreement with previous simulation data for the vapour and liquid coexistence densities from different authors and different simulation techniques can be noticed.

The vapour–liquid coexistence for a CSW potential of ranges $\lambda = 1.25$ and $\lambda = 1.75$ are shown in Figures 7

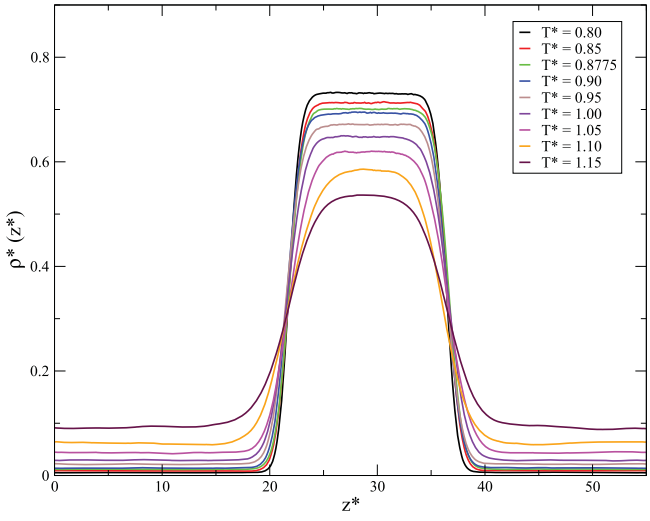

Figure 5. Density profiles for the CSW for $\lambda = 1.5$ for several temperatures (from top to bottom in the liquid region as listed in the figure legend).

Table 2. Vapour–liquid coexistence properties for CSW potentials of different ranges.

T^*	ρ_v^*	ρ_l^*	P_v^*	γ^*
$\lambda = 1.25$				
0.62	0.0239 (09)	0.8597 (54)	0.0137 (14)	
0.64	0.0310 (11)	0.8387 (69)	0.0173 (11)	
0.66	0.0391 (14)	0.8213 (61)	0.0219 (17)	
0.70	0.0696 (18)	0.7567 (43)	0.0355 (19)	
$\lambda = 1.5$				
0.80	0.0057 (05)	0.7310 (39)	0.0040 (16)	0.58 (1)
0.85	0.0092 (05)	0.7130 (39)	0.0070 (15)	0.49 (1)
0.8774	0.0120 (06)	0.7011 (29)	0.0097 (21)	0.45 (1)
0.90	0.0144 (07)	0.6932 (38)	0.0106 (21)	0.43 (1)
0.95	0.0217 (07)	0.6713 (38)	0.0156 (24)	0.35 (1)
1.00	0.0292 (08)	0.6477 (34)	0.0242 (21)	0.27 (1)
1.05	0.0438 (12)	0.6182 (33)	0.0351 (25)	0.20 (1)
1.10	0.0618 (20)	0.5828 (35)	0.0478 (18)	0.14 (1)
1.15	0.0917 (23)	0.5342 (27)	0.0646 (12)	0.07 (1)
$\lambda = 1.75$				
1.20	0.0084 (04)	0.6649 (37)	0.0090 (35)	
1.40	0.0245 (08)	0.5928 (38)	0.0283 (31)	
1.60	0.0582 (13)	0.5083 (34)	0.0628 (32)	

Notes: Numbers in parentheses indicate the standard deviation of the properties in the last two digits, except for the reduced surface tension, γ^*, for which the error is in the last digit. The errors on the surface tensions represent the error of most of the cases from 4 independent runs.

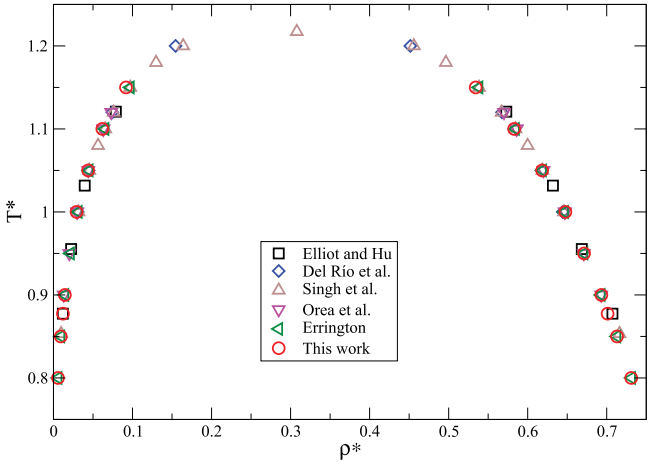

Figure 6. Vapour–liquid phase diagram for an SW potential of range $\lambda = 1.5$. CSW results (circles) and SW simulation data from [38] (squares), [41] (diamonds), [44] (triangles up), [43] (triangles down) and [91] (triangles left) are presented. Error bars are smaller than symbol sizes.

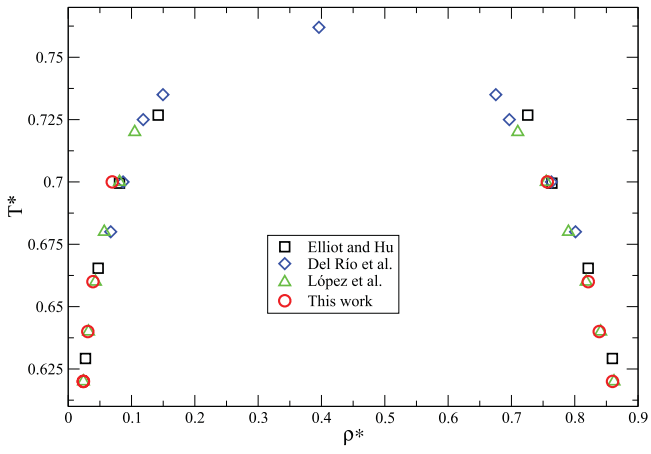

Figure 7. Vapour–liquid phase diagram for an SW potential of range $\lambda = 1.25$ as obtained in this work for the CSW potential (circles) and SW simulation data from [38] (squares), [41] (diamonds) and [49] (triangles). Error bars are smaller than symbol sizes.

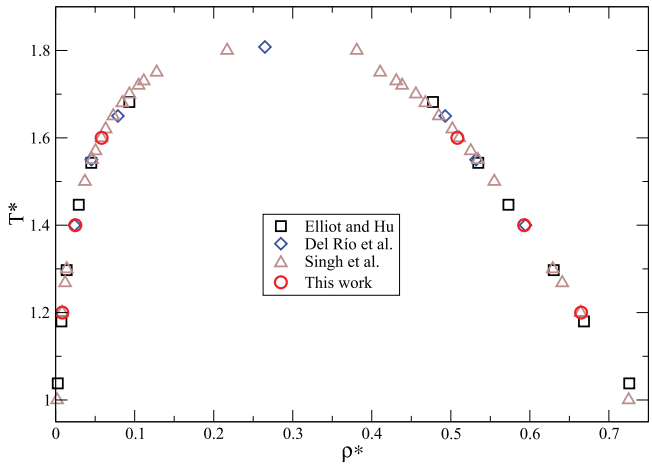

Figure 8. Vapour–liquid coexistence for an SW potential of range $\lambda = 1.75$. CSW potential (circles) and SW simulation data from [38] (squares), [41] (diamonds) and [44] (triangles up) are presented. Error bars are smaller than symbol sizes.

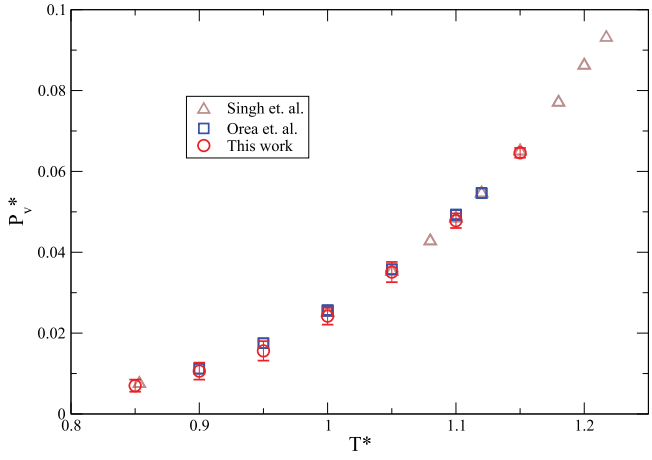

Figure 9. Reduced vapour pressures for an SW potential of range $\lambda = 1.5$. Simulation predictions for the CSW potential are shown (circles). Data for the SW potential from [43] (squares) and [44] (triangles up) are included.

and 8, respectively. The agreement of the simulation data obtained in this work and available simulation data of other authors is good for the states presented.

Reduced vapour pressures were computed using the *zz*-component of the tensor pressure, $P_v^* = P_{zz}^*$, for CSW $\lambda = 1.5$. As can be noticed from Figure 9 the simulated pressures are in agreement with MC data from [43,44]. The simulation vapour pressures are included in Table 2. The standard deviations were obtained, after the first 0.5 ns, by using the averages of 10 sub-blocks of 0.35 ns each .

Lastly, we have carried out longer simulations of 20 ns to compute the surface tension of a CSW potential of range $\lambda = 1.5$. This property was obtained, as mentioned in Section 3, from the pressure components (Equation (4)) which were averaged every 4 ns. The final mean surface tensions are presented in Table 2, plotted in Figure 10 and contrasted with previous results for an SW fluid. As can be seen the predictions are in a good agreement with the available simulation data.

It is important to remark that although this CSW potential reproduces quantitatively well the discontinuous SW potential properties, it is restricted to the use of low time step values (0.0001 ps) and that makes the calculations somewhat more expensive from a computational point of view.

However, there could be also interest in using this continuous potential expression using lower exponent values, like, for instance, the ones shown in Figure 1, (400,400), which also captures the essential characteristics of the SW potential and can be studied using a time step one order of magnitude greater (see Appendix 2).

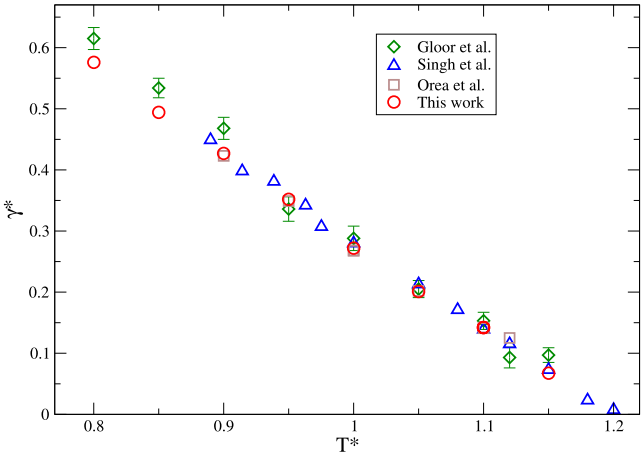

Figure 10. Surface tension for an SW potential of range $\lambda = 1.5$. The corresponding CSW potential results are shown with circles. SW simulation data from [43] (squares), [44] (triangles) and [46] (diamonds) are included.

5. Corollary

As a consequence of this work, we found the following continuous version of the square-shoulder (CSS) potential that, as mentioned in Section 1, is also a very interesting simple discrete potential that exhibits a rich phase behaviour that can model real simple and complex systems [28]. The CSS potential can be written as

$$u_{CSS}(x) = \frac{1}{2}\left(\left(\frac{1}{x}\right)^n - \frac{1-\mathrm{e}^{-m(x-a)(x-\lambda)}}{1+\mathrm{e}^{-m(x-a)(x-\lambda)}} + 1\right), \quad (5)$$

where $a = 0.99$, $n = 2500$ and $m = 20000$. A version of this CSW potential can be found in Figure 11 where it is compared with an SS potential of range $\lambda = 1.5$. As can be noticed both potentials almost overlap. We also included another set of parameters for a softer version of the CSS potential. The exploration of the phase diagram for this potential will be of interest in future studies.

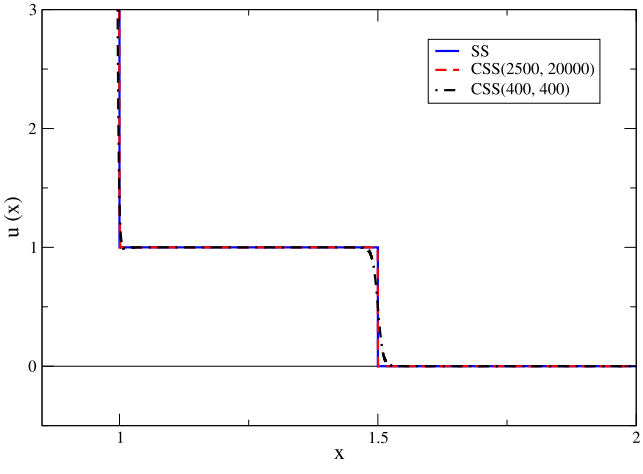

Figure 11. CSS and SS potentials for the case of SS range $\lambda = 1.5$. In this figure, for the CSS potential we have used $a = 0.99$, $n = 2500$, $m = 20000$ and as can be seen it almost overlap with the SS potential. To show an example of a softer version of the CSW potential we have also included a case with $a = 0.99$, $n = 400$ and $m = 400$.

6. Conclusions

We have presented a simple continuous mathematical expression for the discontinuous SW potential of variable range ($\lambda \geq 1.05$). MD simulations were used with this potential and their predictions were compared with available simulation data (single-state thermodynamic properties (gas, liquid and solid), vapour–liquid phase diagram and surface tension) and their performance were good. We expect that this continuous version of the SW potential can be useful to overcome the difficulties of treating discontinuous potentials in statistical mechanics problems, such as in conventional MD simulations.

Acknowledgements

It is a pleasure to contribute to this special issue dedicated to Daan Frenkel as we have learned so much along these years from his books, papers and important contribution to the area of the computer simulation of fluids.

Disclosure statement

No potential conflict of interest was reported by the authors.

Funding

I. M. Zerón is grateful for the Ph.D. scholarship provided by CONACYT (México). C. Vega would like to thank Project FIS2016-78117-P (Ministerio de Economía y Competividad) for funding. A. L. Benavides thanks the University of Guanajuato under grants 227/2018 of the Convocatoria Institucional de Investigación Científica (CIIC) 2018 and 876/2016-2017. National Laboratory UG-UAA-Conacyt (Consejo Nacional de Ciencia y Tecnología) (123732) is also acknowledged for computing resources.

References

[1] F. del Río and L. Lira, Mol. Phys. **61**, 275 (1987).
[2] F. del Río and L. Lira, J. Chem. Phys. **87**, 7179 (1987).
[3] A.L. Benavides and F. del Río, Mol. Phys. **68**, 983 (1989).
[4] A.L. Benavides and A. Gil-Villegas, Mol. Phys. **97**, 1225 (1999).
[5] J. Chang and S.I. Sandler, Mol. Phys. **81**, 745 (1994).
[6] A. Vidales, A.L. Benavides and A. Gil-Villegas, Mol. Phys. **99**, 703 (2001).
[7] G.A. Chapela, F. del Río, A.L. Benavides and J. Alejandre, J. Chem. Phys. **133**, 234107 (2010).
[8] L.A. Cervantes, G. Jaime-Mu noz, A.L. Benavides, J. Torres-Arenas and F. Sastre, J. Chem. Phys. **142**, 114501 (2015).

[9] I. M. Zerón, L.A. Padilla, F. Gámez, J. Torres-Arenas and A.L. Benavides, J. Mol. Liq. **229**, 125 (2017).
[10] A. Gil-Villegas, A. Galindo, P.J. Whitehead, S.J. Mills, G. Jackson and A.N. Burgess, J. Chem. Phys. **106**, 4168 (1997).
[11] A. Galindo, L.A. Davies, A. Gil-Villegas and G. Jackson, Mol. Phys. **93**, 241 (1998).
[12] E. B. El Mendoub , J.-F. Wax , I. Charpentier and N. Jakse, Mol. Phys. **106**, 20 (2008).
[13] F. J. Martínez-Ruiz, F.J. Blas, A. I. Moreno-Ventas Bravo, J. M. Míguez and L.G. MacDowell, Phys. Chem. Chem. Phys. **19**, 12296 (2017).
[14] K.B. Hollingshead and T.M. Truskett, Phys. Rev. E **91**, 043307 (2015).
[15] S.P. Hlushak, P.A. Hlushak and A. Trokhymchuk, J. Chem. Phys. **138**, 164107 (2013).
[16] C. Thomson, L. Lue and M.N. Bannerman, J. Chem. Phys. **140**, 034105 (2014).
[17] M.G. Noro and D. Frenkel, J. Chem. Phys. **113**, 2941 (2000).
[18] A. Gil-Villegas, C. Vega, F. Del Río and A. Malijevsky, Mol. Phys. **86**, 857 (1995).
[19] D. Fiocco, G. Pastore and G. Foffi, J. Phys. Chem. B **114**, 12085 (2010).
[20] M.A. Miller and D. Frenkel, J. Phys. **S16**, 4901 (2004).
[21] N. Kern and D. Frenkel, J. Chem. Phys. **118**, 9882 (2003).
[22] P.G. Bolhuis, A. Stroobants, D. Frenkel and H.N.W. Lekkerkerker, J. Chem. Phys. **107**, 1551 (1997).
[23] P. R. ten Wolde and D. Frenkel, Science **277**, 1975 (1997).
[24] N. E. Valadez Pérez, A.L. Benavides, E. Schöll-Paschinger and R. Casta neda-Priego, J. Chem. Phys. **137**, 084905 (2012).
[25] G. Foffi, G.D. McCullagh, A. Lawlor, E. Zaccarelli, K.A. Dawson, F. Sciortino, P. Tartaglia, D. Pini and G. Stell, Phys. Rev. E **65**, 031407 (2002).
[26] G.J. Pauschenweina and G. Kahl, Soft Mat. **4**, 1396 (2008).
[27] P. Bolhuis and D. Frenkel, J. Phys. **9**, 381 (1997).
[28] H. Pattabhiraman, G. Avvisati and M. Dijkstra, Phys. Rev. Lett. **119**, 157401 (2017).
[29] G. Malescio and G. Pellicane, Nat. Mater. **2**, 97 (2003).
[30] G. Malescio and G. Pellicane, Phys. Rev. E **70**, 021202 (2004).
[31] J. Fornleitner and G. Kahl, J. Phys. **22**, 104118 (2010).
[32] J. C. Armas-Pérez, J. Quintana, G.A. Chapela, E. Velasco and G. Navascués, J. Chem. Phys. **140**, 064503 (2014).
[33] D. Henderson, W.G. Madden and D.D. Fitts, J. Chem. Phys. **64**, 5026 (1976).
[34] D. Henderson, O.H. Scalise and W.R. Smith, J. Chem. Phys. **72**, 2431 (1980).
[35] D.M. Heyes and P.J. Aston, J. Chem. Phys. **97**, 5738 (1992).
[36] L. Vega, E. de Miguel, L.F. Rull, G. Jackson and I.A. McLure, J. Chem. Phys. **96**, 2296 (1992).
[37] E. de Miguel, Phys. Rev. E **55**, 1347 (1997).
[38] J.R. Elliott and L. Hu, J. Chem. Phys. **110**, 3043 (1999).
[39] S. Labík, A. Malijevský, R. Kao, W.R. Smith and F. Del Río, Mol. Phys. **96**, 849 (1999).
[40] G. Orkoulas and A.Z. Panagiotopoulos, J. Chem. Phys. **110**, 1581 (1999).
[41] F. Del Río, E. Ávalos, R. Espíndola , L. F. Rull , G. Jackson and S. Lago, Mol. Phys. **100**, 2531 (2002).
[42] S.B. Kiselev, J.F. Ely, L. Lue and J.R. Elliott, Fluid Phase Equilib. **200**, 121 (2002).
[43] P. Orea, Y. Duda and J. Alejandre, J. Chem. Phys. **118**, 5635 (2003).
[44] J.K. Singh, D.A. Kofke and J.R. Errington, J. Chem. Phys. **119**, 3405 (2003).
[45] P. Orea, Y. Duda, V.C. Weiss, W. Schröer and J. Alejandre, J. Chem. Phys. **120**, 11754 (2004).
[46] G.J. Gloor, G. Jackson, F.J. Blas and E. de Miguel, J. Chem. Phys **123**, 134703 (2005).
[47] B.H. Patel, H. Docherty, S. Varga, A. Galindo and G.C. Maitland, Mol. Phys. **103**, 129 (2005).
[48] D.L. Pagan and J.D. Gunton, J. Chem. Phys. **122**, 184515 (2005).
[49] R. López-Rendón, Y. Reyes and P. Orea, J. Chem. Phys. **125**, 084508 (2006).
[50] R. Espíndola-Heredia, F. del Río and A. Malijevsky, J. Chem. Phys. **130**, 024509 (2009).
[51] Y.T. Pavlyukhin, J. Struct. Chem. **53**, 476 (2012).
[52] J. Jover, A.J. Haslam, A. Galindo, G. Jackson and E. A. Müller, J. Chem. Phys. **137**, 144505 (2012).
[53] H. Neitsch and S.H.L. Klapp, J. Chem. Phys. **138**, 064904 (2013).
[54] J.R. Solana, J. Chem. Phys. **129**, 244502 (2009).
[55] H.J.C. Berendsen, D. van der Spoel and R. van Drunen, Comput. Phys. Commun. **91**, 43 (1995).
[56] E. Lindahl, B. Hess and D. van der Spoel, J. Mol. Model. **7**, 306 (2001).
[57] D. van der Spoel, E. Lindahl, B. Hess, G. Groenhof, A.E. Mark and H.J.C. Berendsen, J. Comput. Chem. **26**, 1701 (2005).
[58] B. Hess, C. Kutzner, D. van der Spoel and E. Lindahl, J. Chem. Theory Comput. **4**, 435 (2008).
[59] S. Pronk, S. Páll, R. Schulz, P. Larsson, P. Bjelkmar, R. Apostolov, M.R. Shirts, J.C. Smith, P.M. Kasson, D. van der Spoel, B. Hess and E. Lindahl, Bioinformatics **29**, 845 (2013).
[60] S. Páll, M.J. Abraham, C. Kutzner, B. Hess and E. Lindahl, Proceedings of EASC 2015 LNCS, **8759,** 3 (2015).
[61] M.J. Abraham, T. Murtola, R. Schulz, S. Páll, J.C. Smith, B. Hess and E. Lindahl, SoftwareX **1**, 19 (2015).
[62] B.R. Brooks, C.L. Brooks, A.D. Mackerell, L. Nilsson, R.J. Petrella, B. Roux, Y. Won, G. Archontis, C. Bartels, S. Boresch, A. Caflisch, L. Caves, Q. Cui, A.R. Dinner, M. Feig, S. Fischer, J. Gao, M. Hodoscek, W. Im, K. Kuczera, T. Lazaridis, J. Ma, V. Ovchinnikov, E. Paci, R.W. Pastor, C.B. Post, J.Z. Pu, M. Schaefer, B. Tidor, R.M. Venable, H.L. Woodcock, X. Wu, W. Yang, D.M. York and M. Karplus, J. Comput. Chem. **30**, 1545 (2009).
[63] I.T. Todorov, W. Smith, K. Trachenko and M.T. Dove, J. Mater. Chem. **16**, 1911 (2006).
[64] H.J. Limbach, A. Arnold, B.A. Mann and C. Holm, Comput. Phys. Commun. **174**, 704 (2006).
[65] J. Roth, F. Gähler and H.R. Trebin, Int. J. Mod. Phys. C **11**, 317 (2000).
[66] S. Plimpton, J. Comput. Phys. **117**, 1 (1995).
[67] C. Niethammer, S. Becker, M. Bernreuther, M. Buchholz, W. Eckhardt, A. Heinecke, S. Werth, H.-J. Bungartz, C.W. Glass, H. Hasse, J. Vrabec and M. Horsch, J. Chem. Theory Comput. **10**, 4455 (2014).

[68] J.C. Phillips, R. Braun, W. Wang, J. Gumbart, E. Tajkhorshid, E. Villa, C. Chipot, R.D. Skeel, L. Kale and K. Schulten, J. Comput. Chem. **26**, 1781 (2005).
[69] P. Ren and J.W. Ponder, J. Phys. Chem. B **107**, 5933 (2003).
[70] J.A. Anderson, C.D. Lorentz and A. Travesst, J. Comput. Phys. **227**, 10 (2008).
[71] J. Glaser, T.D. Nguyen, J.A. Anderson, P. Liu, F. Spiga, J.A. Millan, D.C. Morse and S.C. Glotzer, Comput. Phys. Commun. **192**, 97 (2015).
[72] B.J. Alder and T.E. Wainwright, J. Chem. Phys. **31**, 459 (1959).
[73] G.A. Chapela, S. E. Martínez-Casas and J. Alejandre, Mol. Phys. **53**, 139 (1984).
[74] J. C. Armas-Pérez, J. Quintana-H and G.A. Chapela, J. Chem. Phys. **138**, 044508 (2013).
[75] J. Cui and J.R. Elliott, J. Chem. Phys. **116**, 8625 (2002).
[76] M.N. Bannerman, R. Sargant and L. Lue, J. Comput. Chem. **32**, 3329 (2011).
[77] P. Orea and G. Odriozola, J. Chem. Phys. **138**, 214105 (2013).
[78] L.A. Padilla and A.L. Benavides, J. Chem. Phys. **147**, 034502 (2017).
[79] J.R. Espinosa, E. Sanz, C. Valeriani and C. Vega, J. Chem. Phys. **139**, 144502 (2013).
[80] Y.D. Fomin, N.V. Gribova, V.N. Ryzhov, S.M. Stishov and D. Frenkel, J. Chem. Phys. **129**, 064512 (2008).
[81] N.V. Gribova, Y.D. Fomin, D. Frenkel and V.N. Ryzhov, Phys. Rev. E **79**, 051202 (2009).
[82] G. Franzese, J. Mol. Liq. **136**, 267 (2007).
[83] J.Y. Abraham, S.V. Buldyrev and N. Giovambattista, J. Phys. Chem. B **115**, 14229 (2011).
[84] D. Beeman, J. Comput. Phys. **20**, 130 (1976).
[85] S. Nosé, J. Chem. Phys. **81**, 515 (1984).
[86] G.A. Chape, G. Saville and J.S. Rowlinson, Faraday Discuss. Chem. Soc. **59**, 22 (1975).
[87] G.A. Chapela, G. Saville, S.M. Thompson and J.S. Rowlinson, J. Chem. Soc., Faraday Trans. 2 **73**, 1133 (1977).
[88] Y. Duda, J. Chem. Phys. **130**, 116101 (2009).
[89] L. Acedo and A. Santos, J. Chem. Phys. **115**, 2805 (2001).
[90] D.A. Young and B.J. Alder, J. Chem. Phys. **73**, 2430 (1980).
[91] J.R. Errington, J. Chem. Phys. **118**, 9915 (2003).

Appendices

Appendix 1. Fortran program for the tabulated CSW potential for GROMACS 5.1

```
c  This program generates the GROMACS input file
c  'table_Ar_Ar.xvg', in which the potential CSW and its
c  force have been tabulated.
c  The LJ parameters for Argon are the diameter in nanometres
c  and the energy minimum ϵ in kJ/mol.
program (tabulation CSW)
implicit double precision(a-h,o-z)
dimension u(1000000), rr(1000000), deri(1000000),
     &fuerza(1000000)
open(unit = 3,file = "table_Ar_Ar.xvg",
     &status = "unknown")
sigma = 0.3405d0
xepsilon = 0.996078d0
cero = 0.d0
c  These are the CSW parameters.
c  xlam is the range of the SW potential that we wish to mimic.
xlam = 1.5d0
c  This is the exponent that characterises the softness of the
c  repulsive part of the CSW.
n = 2500
c  This is the exponent that characterises the softness of the
c  attractive part of the CSW potential.
m = 20000
c  Since it is not necessary to evaluate the potential from r = 0
c  we start at r = 0.2
overlap = 0.2d0
c  The spacing gap in the table.
c  The potential will be evaluated every 0.00001, starting at
c  r = 0.2.
dis = 0.00001d0
c  This is the table cutoff reported in the grompp.mdp file in
c  GROMACS see 'User-specified potential functions' from
c  the GROMACS manual.
nsteps = 0.850d0/dis
xn = nsteps
nsteps = nint(xn)
do ir = 1,nsteps+3
c  The number 3 is added to have at least data from r = 0 to
c  r = table  cut-off.
rr(ir) = 0.0d0 + (ir-1.d0)*dis
if (rr(ir).lt.overlap) then
u(ir) = 0.00d0
deri(ir) = 0.0d0
fuerza(ir) = -deri(ir)
write(3,200) rr(ir),cero,cero,u(ir),fuerza(ir),cero,cero
else
x = rr(ir)/sigma
c  Here we start to build the mathematical expression for the
c  CSW potential and its force
arg = -m * (x - xlam) * (x - 1.d0)
if(arg.ge.600.d0) then
c  To avoid computational limits in evaluating big numbers, we
c  have limited the exponential argument. Bigger than this
c  number can generate errors
arg = 600.d0
endif
c  This is the CSW potential
      u(ir) = xepsilon * 0.5d0 * ((1.d0/x) * *n + (1.d0 -
      &dexp(arg))/(1.d0 + dexp(arg)) - 1.d0)
c This is the CSW force
      deri(ir) = xepsilon * 0.5d0 * (1.d0/sigma) * (-n *
      &(1.d0/x) * *(n + 1.d0) + 2.d0 * m * (2.d0 * x - xlam -
      &1.d0) * dexp(arg)/((1.d0 + dexp(arg)) *
      &(1.d0 + dexp(arg))))
fuerza(ir) = - deri(ir)
if (x.gt.xlam) then
c  We selected a criterium to set the rcut of the CSW potential
c  and its force when they differ to zero in 10^-16
if(-u(ir).le.1.d-16) then
u(ir) = cero
endif
if(deri(ir).le.1.d-16) then
fuerza(ir) = cero
endif
endif
```

```
c    These are restrictions of GROMACS 5.1 to handle very
c    small and very big numbers so we fixed the potential and the
c    force to zero for such cases.
if(u(ir).ge.1.d30) then
u(ir) = cero
fuerza(ir) = -cero
endif
if(Abs(fuerza(ir)).lt.1.d-99) then
fuerza(ir) = cero
endif
write(3,200) rr(ir),cero,cero,u(ir),fuerza(ir),cero,cero
endif
enddo
200 format(2x,7(E15.8,4x))
stop
end
```

Appendix 2. Time step and (n, m) optimised selection

The CSW potential depends on n and m parameters (see Figure A1) and these values are related to the steepness around σ and $\lambda\sigma$ of the mimicked SW potential. In MD simulations small time steps are required for potentials that are very steep. We performed NVT MD simulations using 1000 particles at a density $\rho^* = 0.8$ and $T^* = 2$. We analysed different (n, m) parameter sets and to prevent that the simulation crashes due to particle overlapping we needed to test different time steps and we found for the (n, m) cases considered in this work the time step upper limits reported in Table 1.

Note that one needs to decrease the time step by one order of magnitude in going from (600, 600) to (1500, 20000) cases. Doing a more fine time step search for the case selected in this work (2500, 20000), we found that we could use $\delta t = 0.0003$ ps but we decided to use $\delta t = 0.0001$ ps to guarantee not having problems in any of the CSW different states of matter studied.

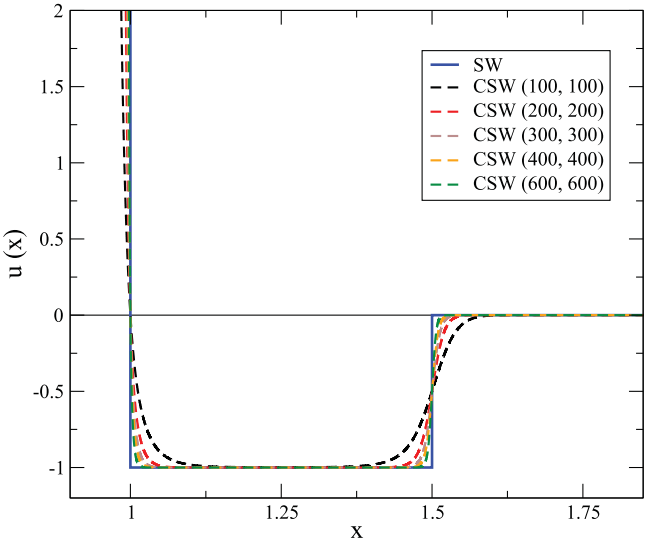

Figure A1. CSW (n, m) and SW potentials for the case $\lambda = 1.5$. The cases (1500, 20000) and (2500, 20000) overlap in this plot with the SW potential. As can be noticed the CSW potential deviates more from the SW potential as one reduces the (n, m) values.

Table 1. Recommended maximum time step to be used with CSW (n, m) potentials to avoid simulation crashes.

CSW potential	Maximum time step (ps)
(100, 100)	0.006
(200, 200)	0.003
(300, 300)	0.002
(400, 400)	0.001
(600, 600)	0.001
(1500, 20000)	0.0003
(2500, 20000)	0.0003

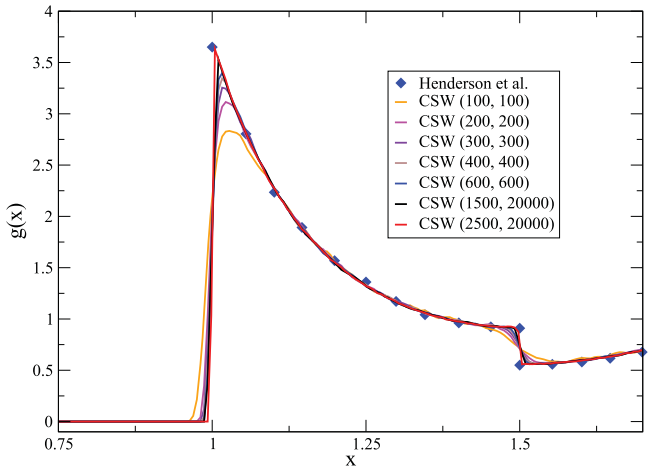

Figure A2. Radial distribution function for several CSW potential cases (n, m) at reduced density $\rho^* = 0.8$ and temperature $T^* = 2$. Simulation data for SW potential of range $\lambda = 1.5$ from [33] are shown with diamond symbols. As can be seen the agreement between the CSW and SW potentials improves using the higher (n, m) values.

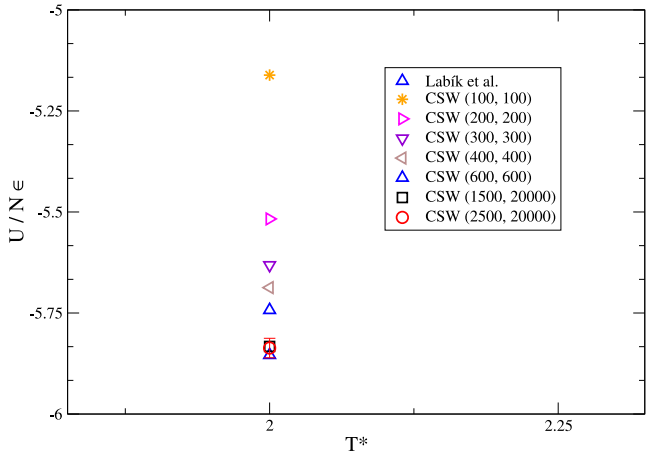

Figure A3. Excess internal energy, $U/N\epsilon$, for several CSW potential (n, m) cases used to mimic the behaviour of an SW potential of range $\lambda = 1.5$ at reduced density $\rho^* = 0.8$ and temperature $T^* = 2$. Target simulation data from [39] is shown with a triangle symbol and CSW data with other symbols (see legend). As can be noticed the agreement between CSW and SW potentials improves as (n, m) values increase.

The selection of the set (2500, 20000) used in this work has been done by analysing the performance of the CSW potential that best mimicked the SW ($\lambda = 1.5$) potential. We selected some target properties: single-state properties (internal energies, pressures and pair correlation functions) and vapour–liquid coexistence densities.

We found that if we want to reproduce accurately the SW potential properties, these (2500, 20000) high values are required. See, for example, Figure A2 that shows the simulated SW pair correlation function obtained by Henderson et al. [33] and different CSW potentials. As can be noticed if one wants to accurately reproduce the first pair correlation peak we need to use around (2500, 20000) values.

Nevertheless, if one is interested in only qualitatively describing an SW behaviour, one can try smaller n and m values (around (600, 600)) and then use an one order of magnitude greater time step as can be seen in Table 1.

Besides, in Figure A3 the internal energy $U/N\epsilon$ for the same thermodynamic state is shown for several CSW cases and the simulation data of [39]. Again the best CSW performance is obtained with the case (2500, 20000).

We did a similar analysis with other properties and found that the CSW potential with (2500, 20000) showed the best performance when compared with the available SW simulation data.